Highlighting research from the State Key Laboratory of Luminescent Materials and Devices, South China University of Technology.

Solution-processable, star-shaped bipolar tetraphenylethene derivatives for the fabrication of efficient nondoped OLEDs

Small molecules possess the merits of finely defined structures and high purity but are generally only suitable for vacuum deposition in fabricating optoelectronic devices because of their poor film-forming ability by solution process. In this work, Zhao, Tang and coworkers prepared a series of solution-processable, star-shaped tetraphenylethene derivatives containing electron-donor and acceptor groups. These luminogens show aggregation-induced emission (AIE) and good film-forming ability, and can be used to fabricate efficient nondoped OLEDs by spin coating technique, indicating their great potential in flexible displays.

As featured in:

See Zujin Zhao, Ben Zhong Tang *et al.*, *J. Mater. Chem. C*, 2016, **4**, 2775.

ROYAL SOCIETY OF CHEMISTRY

www.rsc.org/MaterialsC

Registered charity number: 207890

Journal of Materials Chemistry C

PAPER

View Article Online
View Journal | View Issue

Cite this: J. Mater. Chem. C, 2016, 4, 2775

Solution-processable, star-shaped bipolar tetraphenylethene derivatives for the fabrication of efficient nondoped OLEDs

Long Chen,[a] Chongyang Zhang,[a] Gengwei Lin,[a] Han Nie,[a] Wenwen Luo,[a] Zeyan Zhuang,[a] Siyang Ding,[a] Rongrong Hu,[a] Shi-Jian Su,[a] Fei Huang,[a] Anjun Qin,[a] Zujin Zhao*[a] and Ben Zhong Tang*[ab]

Received 16th September 2015,
Accepted 4th November 2015

DOI: 10.1039/c5tc02949j

www.rsc.org/MaterialsC

Organic light-emitting diodes (OLEDs) based on solution-processable small molecules are attracting intense attention, as such technology combines the merits of low-cost solution processability of polymers and finely defined structural uniformity of small molecules. Small-molecule tetraphenylethene (TPE) derivatives are excellent solid-state light emitters featuring aggregation-induced emission (AIE) characteristics, however those that can be used in solution-processable devices are very rare. To address this issue, herein, a series of novel star-shaped bipolar TPE derivatives are synthesized and characterized. Their thermal stabilities, photophysical properties, electronic structures, electrochemical behaviors, and application in solution-processed OLEDs are investigated systematically. These luminogens exhibit AIE characteristics and excellent fluorescence quantum yields up to 95% in the solid state. Nondoped OLEDs are successfully fabricated through a spin-coating method. The solution-processed OLEDs [ITO (130 nm)/PEDOT:PSS (40 nm)/emitter (70 nm)/TPBi (30 nm)/Ba (4 nm)/Al (120 nm)] adopting star-shaped TPE derivatives as light-emitting layers show peak luminance of 11665 cd m^{-2} and high electroluminescence (EL) efficiencies up to 8.3 cd A^{-1}, 2.6% and 7.5 lm W^{-1}. These results demonstrate a promising avenue towards efficient nondoped OLEDs based on solution-processable AIE-active small molecules.

Introduction

Organic light-emitting diodes (OLEDs) have attracted considerable attention due to their potential applications in flat-panel displays and solid-state lighting after the pioneering work reported by Tang *et al.* in 1987.[1] To date, the most effective method to fabricate OLEDs is vapor deposition under vacuum.[2–5] However, the thermal evaporation process increases the fabrication complexity and brings about very low utilization of expensive light-emitting materials.[6] Solution-involved processes, such as spin-coating and ink-jet printing, are considered to be the best way to improve the efficiency of the process and reduce the production cost.[7,8] In the past few decades, conjugated polymers have dominated the solution-processable electroluminescent materials,[9–11] but they have some disadvantages such as the difficulty in controlling batch-to-batch variation and the impurities in the polymeric materials. In comparison to polymers, small molecules present several intrinsic advantages such as easy synthesis, high purity and defined chemical structure. Therefore, to improve the prospects for the fabrication of large-area and low-cost flat-panel displays and solid-state lighting, employing solution-processable small molecules to make OLEDs is a promising alternative.[12–16] Unfortunately, a large majority of small molecules are designed for vacuum deposition, and are not suitable for solution processing due to their poor film-forming ability and good crystalline properties. To form a smooth and stable film with appropriate thickness, good solubility and high glass-transition temperature (T_g) are required for small-molecule luminescent materials.[17,18] Although some advances on solution-processable small molecules have been achieved recently, progress is still far from the commercial stage, and the most difficult part lies in the design of efficient materials.[17]

In order to fabricate high-performance OLEDs, high photoluminescence (PL) efficiency of the organic luminescent material in solid films is one of the essential factors that must be satisfied.[9,19] However, most conventional luminescent materials are strongly emissive in solutions but suffer from severe

[a] State Key Laboratory of Luminescent Materials and Devices, South China University of Technology, Guangzhou 510640, China. E-mail: mszjzhao@scut.edu.cn
[b] Department of Chemistry, The Hong Kong University of Science and Technology, Clear Water Bay, Kowloon, Hong Kong, China. E-mail: tangbenz@ust.hk

aggregation-caused quenching (ACQ), due to the formation of such detrimental species as excimers or exciplexes when aggregated.[20] Various chemical, physical and engineering approaches have been proposed to mitigate the ACQ effect,[21,22] but they often result in other adverse effects.[23] The intriguing aggregation-induced emission (AIE) phenomenon refers to certain luminogens which are nonfluorescent in solutions but become strongly emissive when aggregated in poor solvents or fabricated as thin films,[24–26] which opposes the ACQ effect. Through the combination of AIE-active units and conventional ACQ building blocks, various luminescent materials with excellent solid-state efficiencies have been developed and function outstandingly as light-emitting layers for nondoped OLEDs, demonstrating a promising approach to solve the ACQ problem of conventional light-emitting materials.[2,19,27–37]

So far, a great many luminogens with AIE features have been reported as efficient electroluminescent materials, but solution-processable AIE materials remain rare and are hardly developed in OLEDs. In our previous study, we developed a series of solid-state luminescent materials based on a popular AIE unit, tetraphenylethene (TPE), and high-performance nondoped OLEDs were attained using these materials as light-emitting layers. We found that unsymmetrical linear TPE derivatives, carrying diphenylamino and dimesitylboryl as electron donor and acceptor groups, were excellent light emitters for OLEDs, but they could only be processed by vapor deposition because of the poor film-forming ability upon spin-coating.[19] Herein, we report the synthesis and characterization of three tailored star-shaped TPE derivatives with different proportions of donor and acceptor groups, in which TPE is adopted as an AIE-active bridge, and diphenylamino and dimesitylboryl groups serve as electron donor and acceptor, respectively. The ratio of electron donor and acceptor groups is adjusted to achieve a good balance for electron and hole transport. The thermal, photophysical, electronic, electrochemical, and electroluminescent properties of the novel star-shaped TPE derivatives are investigated. All the luminogens possess AIE characteristics and are highly fluorescent in solid films with high PL efficiencies up to 95%. Furthermore, these luminogens can form smooth films by the spin-coating method, and are morphologically stable with high T_g values of 173–190 °C. The nondoped OLEDs fabricated from these new luminogens by a solution process show excellent performance, with electroluminescence (EL) efficiencies as high as 8.3 cd A^{-1}, 2.6% and 7.5 lm W^{-1}. These results indicate that the precisely designed star-shaped TPE derivatives are promising solution-processable candidates for efficient nondoped OLEDs.

Results and discussion

Synthesis

Recently, we reported the synthesis and application of unsymmetrical linear TPE derivatives bearing diphenylamino and dimesitylboryl as donor and acceptor groups, respectively. However, the final products were mixtures of *cis*- and *trans*-isomers that could hardly be separated due to their similar structures and polarity. Although the *cis*- and *trans*-isomers showed similar chemical and photophysical properties, it was not ideal to attempt to perform a straightforward analysis of structure–property relationship based on stereorandom products. In this work, a series of novel star-shaped TPE derivatives (Scheme 1) with defined chemical structures were successfully prepared according to the synthesis routes outlined in Scheme 2. The detailed procedures and characterization data are given in the Experimental section. Briefly, compounds **4**,[38] **7**,[2] **9**,[39] and **10**[19] were prepared according to the methods described in the literature. Bis[4′-(dimesitylboranyl)-(1,1′-biphenyl)-4-yl]methanone (**8**) was obtained through the Suzuki coupling of **6** with **7**. The final products, TPE-2PN2PB and TPE-4PB, were synthesized by McMurry coupling of **4** with **8**. The intermediate **12** was also obtained through McMurry coupling of 4,4′-dibromobenzophenone (**3**) with **11**. The Suzuki coupling of **12** with **10** furnished TPE-PN3PB. These novel star-shaped TPE derivatives were fully characterized by NMR and mass spectroscopies, which verified their molecular structures. They are soluble in common organic solvents including THF, chloroform, dichloromethane, toluene, *etc.*, but can hardly dissolve in water.

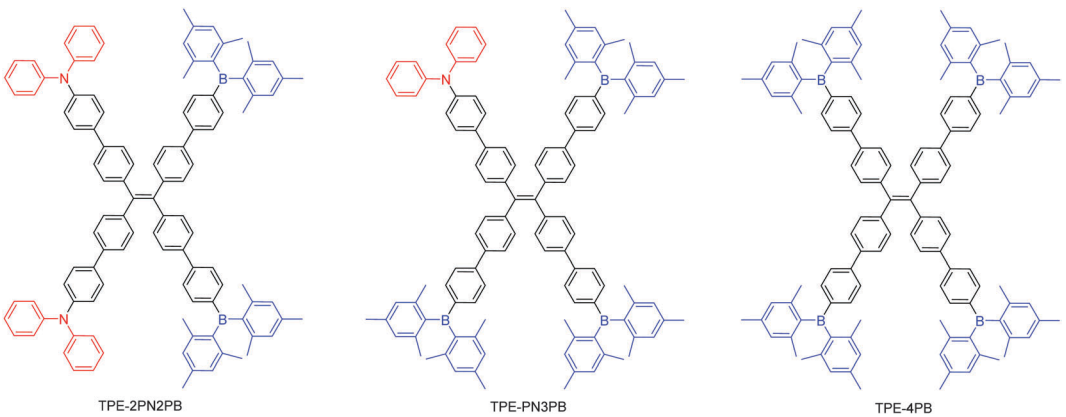

Scheme 1 Chemical structures of star-shaped TPE derivatives, TPE-2PN2PB, TPE-PN3PB and TPE-4PB.

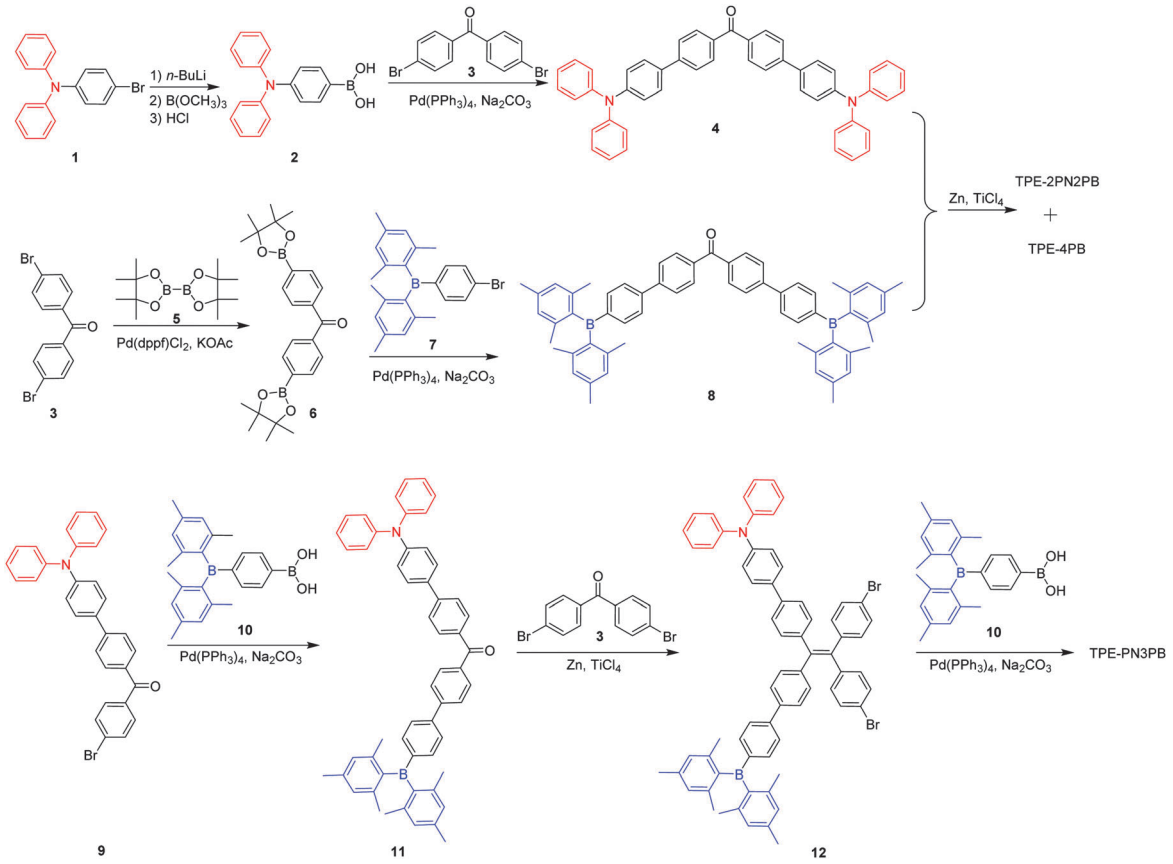

Scheme 2 Synthesis routes to TPE-2PN2PB, TPE-PN3PB and TPE-4PB.

Optical properties

The photophysical properties of these star-shaped TPE derivatives were measured using UV-visible absorption and PL spectroscopies. The absorption spectra of these new luminogens in dilute THF solutions (10 μM) are shown in Fig. 1A. The spectral profiles of TPE-2PN2PB, TPE-PN3PB and TPE-4PB are similar, with absorption maxima at 350, 348 and 346 nm, respectively, and similar molar absorptivities. The PL spectra of these TPE derivatives in dilute THF solutions (10 μM) are shown in Table 1. Like most TPE derivatives, these new luminogens exhibit weak emissions in the solution state. Only weak PL signals with emission maxima at 526, 533 and 525 nm are recorded for TPE-2PN2PB, TPE-PN3PB and TPE-4PB, respectively. The fluorescence quantum yields (Φ_F) for TPE-2PN2PB, TPE-PN3PB and TPE-4PB in dilute THF solutions are as low as 2.8, 3.7 and 4.5%, respectively, measured by an integrating sphere, which confirms that they are practically very weak emitters when dissolved in good solvents. They become highly emissive in the solid state, and the films of TPE-2PN2PB, TPE-PN3PB and TPE-4PB fluoresce intensely peaking at 540, 528 and 524 nm, respectively (Fig. 1B). The Φ_F values of TPE-2PN2PB, TPE-PN3PB and TPE-4PB in the solid state are as high as 95, 92 and 91%, respectively, determined by an integrating sphere, revealing that they feature AIE characteristics and are excellent solid-state emitters.

Table 1 Optical, electronic and thermal properties of TPE-2PN2PB, TPE-PN3PB and TPE-4PB

Compounds	λ_{abs}[a] (nm)	λ_{em}[a] (nm)		Φ_F[c] (%)		T_g/T_d (°C)	HOMO/LUMO[d] (eV)	E_g (eV)
		THF	Film[b]	THF	Solid			
TPE-2PN2PB	350	526	540	2.8	95	190/284	−5.32/−2.77	2.55
TPE-PN3PB	348	533	528	3.7	92	183/365	−5.32/−2.79	2.53
TPE-4PB	346	525	524	4.5	91	173/276	−5.63/−3.03	2.60

[a] Measured in THF. [b] Spin-coated film. [c] Absolute fluorescence quantum yield determined by a calibrated integrating sphere. [d] Determined by cyclic voltammetry.

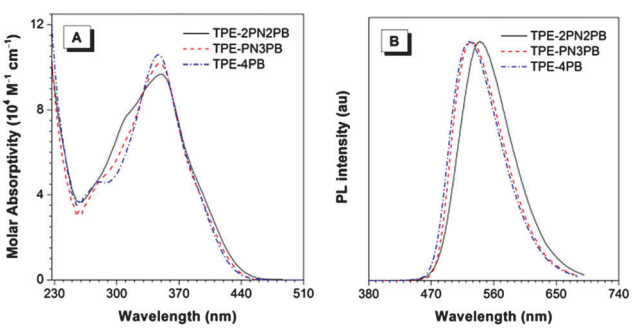

Fig. 1 (A) Absorption (in THF solutions) and (B) PL spectra (in films) of TPE-2PN2PB, TPE-PN3PB and TPE-4PB. Excitation wavelength: 360 nm.

The AIE characteristics of TPE-2PN2PB, TPE-PN3PB and TPE-4PB are further verified by their emission behaviors in THF/water mixtures. Fig. 2A illustrates the PL spectra of TPE-2PN2PB in THF/water mixtures as an example. It can be seen that the emission is weak when the water content is low, but it enhances notably when the water content becomes high. Similar emission behaviors are also recorded for TPE-PN3PB and TPE-4PB in THF/water mixtures (Fig. 2B and C). Since TPE-2PN2PB, TPE-PN3PB and TPE-4PB are insoluble in water, their molecules must have aggregated in aqueous media. The intramolecular rotation that is active in the solution state is restricted due to steric hindrance in the condensed phase. The nonradiative relaxation channel is thus blocked and the radiative decay of the excited state is promoted, rendering these luminogens highly emissive in the solid state. These results further manifest that these novel star-shaped TPE derivatives are AIE-active.

Thermal and morphological properties

The thermal properties of these star-shaped luminogens were evaluated by thermogravimetric analysis (TGA) and differential scanning calorimetry (DSC) (Fig. 3). It is found that they have good thermal stability with decomposition temperatures (T_d) of 276–365 °C, according to 5% loss of initial weight. The results demonstrate that they are thermally stable and able to function steadily as active layers in OLEDs. High T_g values of 173–190 °C are also recorded from these star-shaped TPE derivatives, which are much higher than those of their linear counterparts[19]

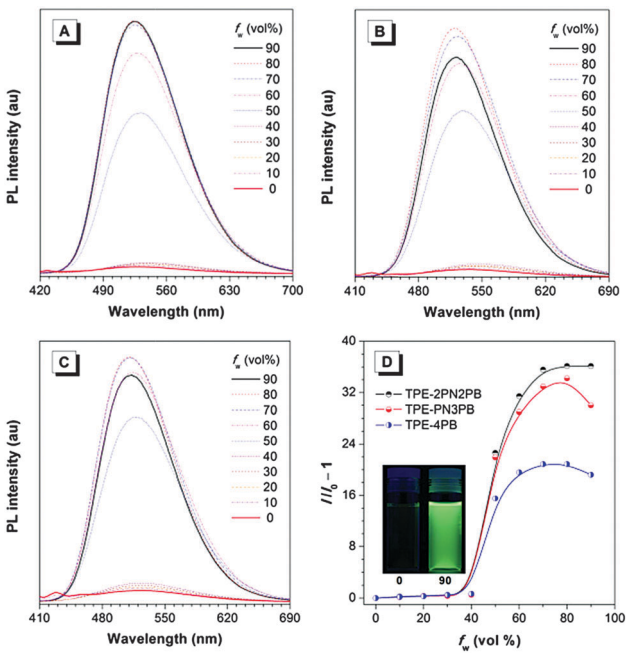

Fig. 2 PL spectra of (A) TPE-2PN2PB, (B) TPE-PN3PB and (C) TPE-4PB in THF/water mixtures with different water fractions (f_w). (D) Plot of ($I/I_0 - 1$) values *versus* water fractions in THF/water mixtures of TPE-2PN2PB, TPE-PN3PB and TPE-4PB. I_0 is the PL intensity in pure THF solution. Inset: photo of TPE-2PN2PB in THF/water mixtures (f_w = 0 and 90%), taken under the illumination of a UV lamp (365 nm).

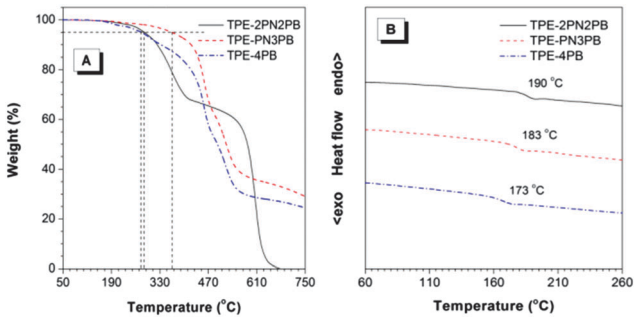

Fig. 3 (A) TGA and (B) DSC curves of TPE-2PN2PB, TPE-PN3PB and TPE-4PB, recorded under nitrogen at a heating rate of 10 °C min^{-1}.

as a result of the nonplanar molecular structure and the enlarged molecular size. Their film-forming properties were also investigated by atomic force microscopy (AFM) as they are important to device performance. As shown in Fig. 4, the AFM images of solution-processed films reveal the smooth and homogeneous film morphologies with very small values of root-mean-square (RMS) roughness of 0.46, 0.51 and 0.54 nm for TPE-2PN2PB, TPE-PN3PB and TPE-4PB, respectively. These results demonstrate that TPE-2PN2PB, TPE-PN3PB and TPE-4PB are all thermally stable and have good film-forming ability by a solution process.

Electronic structure

To gain a deep insight into the electronic structures of these star-shaped TPE derivatives, the optimized molecular structures and spatial distributions of HOMOs and LUMOs were calculated with the density function theory (DFT) method with a B3LYP/6-31G(d) basis set using the Gaussian 09 package. In TPE-2PN2PB and TPE-PN3PB, the diphenylamino groups are occupied by the HOMOs, while the dimesitylboryl groups contribute notably to the LUMOs (Fig. 5). In both luminogens, the HOMOs and LUMOs are almost separated, which is attributed to the different energy levels of electron-rich diphenylamino groups and electron-poor dimesitylboryl groups. The twisted conformation also weakens the electronic coupling between building blocks and results in ineffective conjugation. Hence, the donor–acceptor (D–A) interaction is weak, giving a small dipole moment in the excited state.[19] On the one hand, the relatively weak D–A interaction brings about increased PL and EL efficiencies by virtue of the suppression of nonradiative relaxation.[40,41] On the other hand, it is preferable for efficient

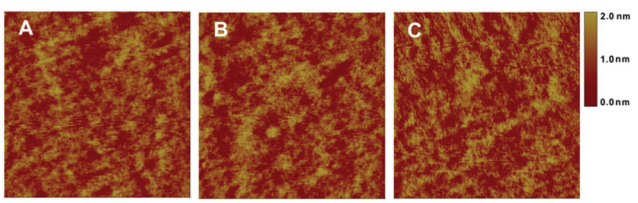

Fig. 4 AFM topographic images (5 × 5 μm) of the solution-processed (A) TPE-2PN2PB, (B) TPE-PN3PB and (C) TPE-4PB films on the ITO substrate pre-spin-coated with PEDOT:PSS.

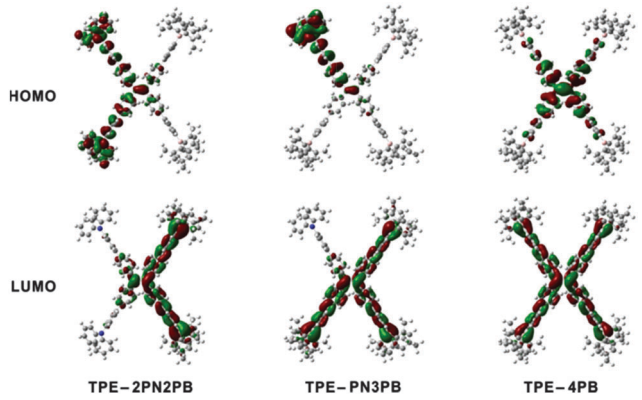

Fig. 5 B3LYP/6-31G(d) calculated molecular orbital amplitude plots of HOMOs and LUMOs of TPE-2PN2PB, TPE-PN3PB and TPE-4PB.

injection and transport of holes and electrons in the donor and acceptor, respectively, which is beneficial to charge balance and exciton recombination in devices.[42] Significant contributions from the boron centers can also be observed in the LUMO of TPE-4PB, and its electronic cloud of LUMO can delocalize to the TPE core through the conjugation of phenyl rings. Such a distinctive electronic structure results in a low LUMO energy level, which could be favorable for electron injection and transport in TPE-4PB.

Electrochemical properties

To evaluate the energy levels of the star-shaped luminogens, the electrochemical properties were investigated by cyclic voltammetry (CV) in dichloromethane solution with 0.1 M tetrabutylammonium hexafluorophosphate as the supporting electrolyte at a scan rate of 100 mV s^{-1} using platinum as the working electrode and saturated calomel electrode (SCE) as the reference electrode. The cyclic voltammograms of TPE-2PN2PB, TPE-PN3PB and TPE-4PB are given in Fig. 6. The diphenylamino-free TPE-4PB exhibits a quasi-reversible oxidation process, with an onset potential at 1.23 V. In contrast, the introduction of electron-donating diphenylamino groups in TPE-2PN2PB and TPE-PN3PB leads to

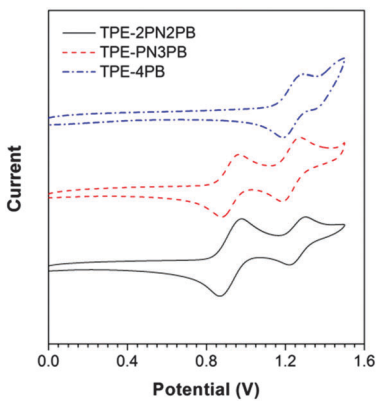

Fig. 6 Cyclic voltammograms of TPE-2PN2PB, TPE-PN3PB and TPE-4PB, measured in dichloromethane containing 0.1 M tetra-*n*-butylammonium hexafluorophosphate. Scan rate: 100 mV s^{-1}.

an extra quasi-reversible oxidation process, with an onset potential at 0.92 V, which implies that the incorporation of the electron-donating diphenylamino group can remarkably decrease the oxidation potential of the luminogen. The energy levels of HOMO [HOMO = $-(4.4 + E_{onset})$] and LUMO [LUMO = HOMO + E_g] are thus determined by the onset potential of oxidation (E_{onset}) and the optical band gap. The HOMO energy level of TPE-4PB is calculated to be −5.63 eV, while those of TPE-2PN2PB and TPE-PN3PB are as high as −5.32 eV. The quite similar HOMO energy levels of TPE-2PN2PB and TPE-PN3PB to that of PEDOT:PSS (−5.2 eV)[43] indicate that hole injection is favored from PEDOT:PSS to both luminogens. The LUMO energy levels of TPE-2PN2PB and TPE-PN3PB are calculated to be −2.77 and −2.79 eV, respectively, while that of TPE-4PB is much lower (−3.03 eV). The LUMO energy levels of these luminogens are lower than that of 1,3,5-tris(*N*-phenylbenzimidazol-2-yl)benzene (TPBi, −2.7 eV),[44] which may facilitate electron transport in the emitting layer.

Electroluminescence

Given the high thermal stability and excellent solid-state emission efficiency, TPE-2PN2PB, TPE-PN3PB and TPE-4PB were subjected to EL study in solution-processed nondoped OLEDs. Trilayer solution-processed OLEDs with a configuration of ITO (130 nm)/PEDOT:PSS (40 nm)/EML (70 nm)/TPBi (30 nm)/Ba (4 nm)/Al (120 nm) were fabricated, in which TPE-2PN2PB, TPE-PN3PB and TPE-4PB served as the light-emitting layer (EML), PEDOT:PSS functioned as the hole-transporting layer (HTL) and TPBi acted as the electron-transporting layer (ETL). The devices exhibit similar EL emissions to the PL emissions of their films. For instance, the EL spectrum of TPE-2PN2PB with a peak at 543 nm (Fig. 7A) is almost identical to the PL spectrum of its film (540 nm), indicating that the exciton recombination zone has been confined inside the light-emitting layer. The current density–voltage–luminance characteristics and efficiency curves of devices are depicted in Fig. 7 and the relevant performance data are summarized in Table 2. The devices based on TPE-2PN2PB and TPE-PN3PB both show low turn-on voltages at 3.4 V, which resulted from the similar energy levels of their HOMOs and LUMOs. The maximum luminance (L_{max}) of the device based on TPE-2PN2PB is as high as 11 665 cd m^{-2} and that of TPE-PN3PB can also reach 7290 cd m^{-2}. Fig. 7C depicts the current efficiency (η_c) as a function of luminance for devices based on these luminogens. Excellent maximum current, external quantum and power efficiencies (η_p) are achieved by devices based on TPE-2PN2PB (8.3 cd A^{-1}, 2.6% and 7.5 lm W^{-1}) and TPE-PN3PB (6.3 cd A^{-1}, 2.1% and 5.9 lm W^{-1}). The values are much better than the reported solution-processable AIE luminogens (*e.g.* 2618 cd m^{-2}, 4.55 cd A^{-1} and 2.17%).[48] Significantly, the devices based on TPE-2PN2PB and TPE-PN3PB show slight EL efficiency roll-off as the luminance increases, and high current efficiencies of 6.2 cd A^{-1} and 4.6 cd A^{-1}, respectively, are achieved at a luminance of 1000 cd m^{-2}. These results demonstrate the great potential of TPE-2PN2PB and TPE-PN3PB as light emitters for solution-processed nondoped OLEDs. However, the device

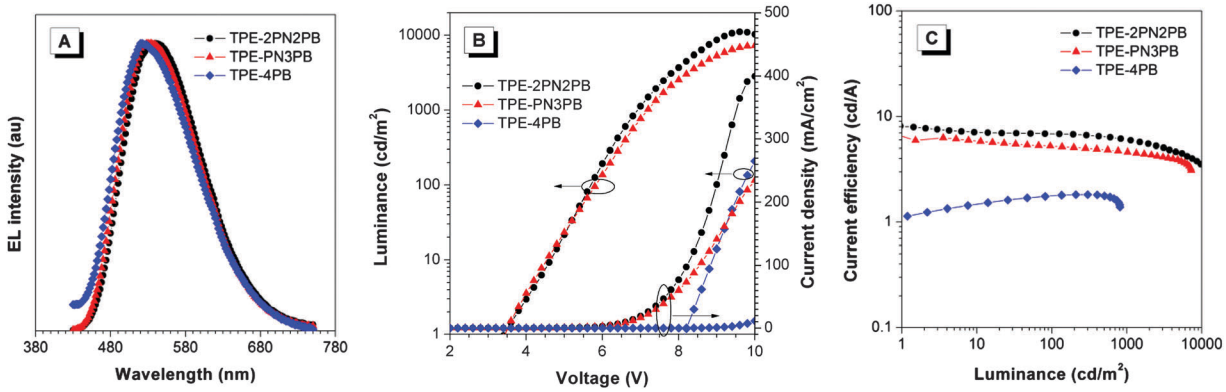

Fig. 7 (A) EL spectra, (B) current density–voltage–luminance characteristics, and (C) current efficiency *vs.* luminance in EL devices of TPE-2PN2PB, TPE-PN3PB and TPE-4PB. Device configuration: ITO (130 nm)/PEDOT:PSS (40 nm)/EML (70 nm)/TPBi (30 nm)/Ba (4 nm)/Al (120 nm).

Table 2 EL performances of solution-processed OLEDs based on TPE-2PN2PB, TPE-PN3PB and TPE-4PB

Emitters	λ_{EL}[a] (nm)	V_{on}[b] (V)	L_{max}[c] (cd m^{-2})	η_c[d] (cd A^{-1})	η_{ext}[e] (%)	η_p[f] (lm W^{-1})	$\eta_{c,1000}$[g] (cd A^{-1})	CIE[h] (x, y)
TPE-2PN2PB	543	3.4	11 665	8.3	2.6	7.5	6.2	0.37, 0.54
TPE-PN3PB	532	3.4	7290	6.3	2.1	5.9	4.6	0.35, 0.53
TPE-4PB	521	8.1	838	1.8	0.6	0.6	—	0.34, 0.50

[a] λ_{EL} = EL maximum. [b] V_{on} = turn-on voltage at 1 cd m^{-2}. [c] L_{max} = maximum luminance. [d] η_c = maximum current efficiency. [e] η_{ext} = maximum external quantum efficiency. [f] η_p = maximum power efficiency. [g] $\eta_{c,1000}$ = current efficiency at 1000 cd m^{-2}. [h] CIE = Commission Internationale de l'Eclairage coordinates. Device configuration: ITO (130 nm)/PEDOT:PSS (40 nm)/EML (70 nm)/TPBi (30 nm)/Ba (4 nm)/Al (120 nm).

constructed using TPE-4PB shows a noticeable deterioration in performance. Fig. 7B shows that the device based on TPE-4PB is turned on at a very high voltage of 8.1 V and its maximum luminance is only 838 cd m^{-2}. The η_c, η_{ext} and η_p of the device based on TPE-4PB can only reach 1.8 cd A^{-1}, 0.6% and 0.6 lm W^{-1}, being much lower than those of TPE-2PN2PB and TPE-PN3PB, which should be attributed to the imbalance of holes and electrons in the emitting layer.

TPE-2PN2PB and TPE-PN3PB have very similar HOMO energy levels to the hole-transporting layer of PEDOT:PSS, and similar LUMO energy level (−2.77 and −2.79 eV) to the electron-transporting layer of TPBi (−2.7 eV). As a result, both hole and electron injection is favorable from the charge-transporting layers to the light-emitting layer for devices based on TPE-2PN2PB or TPE-PN3PB, which can be confirmed by their low turn-on voltages. In addition, the incorporation of electron D–A combination in TPE-2PN2PB and TPE-PN3PB assures their excellent hole and electron transport abilities, which improves the exciton recombination efficiencies due to the balance of holes and electrons.[45–47] However, in the device based on TPE-4PB, the drastically lowered HOMO (−5.63 eV) and LUMO (−3.03 eV) energy levels render difficult hole injection but facile electron injection, which upsets the balance of holes and electrons, and thus has an adverse effect on its device performance.

Conclusions

In this work, we demonstrate efficient nondoped OLEDs fabricated with solution-processable bipolar small-molecule luminescent materials. Three thermally stable star-shaped TPE derivatives (TPE-2PN2PB, TPE-PN3PB and TPE-4PB) are successfully synthesized and fully characterized. They are weakly fluorescent in solution but become highly emissive in the solid state, presenting AIE characteristics. Thanks to their good film-forming abilities, these truly solution-processable AIE luminogens have been used as light-emitting materials in efficient nondoped OLEDs, which afford a high EL efficiency of 8.3 cd A^{-1}. To the best of our knowledge, TPE-2PN2PB and TPE-PN3PB are among the best solution-processable small-molecule luminogens used in nondoped OLEDs.[48–51] It should also be noted that the devices have not yet been optimized thoroughly. Given their excellent optoelectronic properties, highly efficient solution-processed OLEDs are expectable *via* device engineering.

Experimental section

Materials and instruments

Tetrahydrofuran (THF) was distilled from sodium benzophenone ketyl under dry nitrogen immediately prior to use. Compounds **4**, **7**, **9** and **10** were prepared according to the known procedures. All the other chemicals and reagents were purchased from commercial sources and used as received without further purification. NMR spectra were obtained on a Bruker AV 400, 500 or 600 spectrometer. High resolution mass spectra (HRMS) were recorded on a GCT premier CAB048 mass spectrometer operating in MALDI-TOF mode. The ground-state geometries were optimized using the density functional with the B3LYP hybrid functional at the basis set level of 6-31G(d). All the calculations

were performed using the Gaussian 09 package. UV-visible absorption spectra were measured on a SHIMADZU UV-2600 spectrophotometer. Fluorescence spectra were recorded on a Horiba Fluoromax-4 fluorescence spectrophotometer. Fluorescence quantum yields were measured using a Hamamatsu absolute PL quantum yield spectrometer C11347 Quantaurus_QY. TGA analysis was carried out on a TA TGA Q5000 and DSC analysis was performed on a DSC Q1000 under dry nitrogen at a heating rate of 10 °C min^{-1}. Cyclic voltammograms were measured on a CHI 610E A14297.

Device fabrication

Patterned indium tin oxide (ITO, 15 Ω $square^{-1}$, 130 nm) coated glass substrates were cleaned in sequence in an ultrasonic bath of acetone, detergent, de-ionized water, and isopropyl alcohol and then were dried at 80 °C in air for more than 3 h. The cleaned ITO substrates were treated with O_2 plasma for 5 min before film coating. A 40 nm layer of poly(3,4-ethylenedioxythiophene)–poly-(styrenesulfonic acid) (PEDOT:PSS) was spin-coated on the ITO substrate in air. These PEDOT:PSS-coated ITO substrates were then transferred into a glove box with a N_2 atmosphere and dried at 120 °C for 20 min to remove residual water. TPE-2PN2PB and TPE-PN3PB dissolved in chlorobenzene, and TPE-4PB dissolved in a mixture of chlorobenzene and chloroform (5 : 1 v/v) were spin-coated on the PEDOT:PSS layer to form a 70 nm light-emitting layer. Then a 30 nm TPBi layer was vacuum-deposited through a shadow mask. Finally, 4 nm Ba and 120 nm Al films were subsequently vacuum-deposited to form the top cathode. Profilometry (Veeco Dektak 150) was used to determine the thickness of the solution-processed organic layer. The thicknesses of vacuum-deposited organic layers and the cathode were monitored upon deposition by using a crystal thickness monitor (Sycon) and calibrated using a Veeco Dektak 150. Current density–voltage–luminance characteristics of the solution-processed light-emitting devices were measured using a Keithley 236 source meter and a calibrated silicon photodiode. Luminance was calibrated by a spectrophotometer (Photo Research, model Spectra Scan PR-705), and the EL spectrum and Commission International de I'Eclairage (CIE) coordinates were simultaneously obtained.

Preparation of nanoaggregates

Stock THF solutions of the luminogens with a concentration of 10^{-4} M were prepared. Aliquots of the stock solution were transferred to 10 mL volumetric flasks. After appropriate amounts of THF were added, water was added dropwise under vigorous stirring to furnish 10^{-5} M solutions with different water contents (0–90 vol%). The PL measurements of the resultant solutions were then performed immediately.

Synthesis

Bis[4-(4,4,5,5-tetramethyl-1,3,2-dioxaborolan-2-yl)phenyl]-methanone (6). Into a 250 mL two-necked round bottom flask with a reflux condenser were placed **3** (3.40 g, 10.0 mmol), **5** (6.10 g, 24.0 mmol), Pd(dppf)Cl_2 (440 mg, 0.60 mmol) and potassium acetate (2.94 g, 30.0 mmol). The flask was evacuated under vacuum and flushed with dry nitrogen three times and then 1,4-dioxane (80 mL) was added. The reaction mixture was heated to reflux for 24 h. After cooling to room temperature, the mixture was poured into water and extracted with dichloromethane three times. The combined organic layers were dried over anhydrous magnesium sulfate. After filtration and solvent evaporation, the crude product was purified by silica-gel column chromatography. White solid compound **6** was obtained in 86% yield. ^{1}H NMR (600 MHz, $CDCl_3$), δ (ppm): 7.92 (d, 4H, J = 7.8 Hz), 7.77 (d, 4H, J = 7.8 Hz), 1.37 (s, 24H). ^{13}C NMR (150 MHz, $CDCl_3$), δ (ppm): 197.07, 139.65, 134.57, 129.07, 84.21, 24.90. HRMS ($C_{25}H_{32}B_2O_5$): m/z 435.2576 [M^+, calcd 434.2436].

Bis[4′-(dimesitylboranyl)-(1,1′-biphenyl)-4-yl]methanone (8). Into a 250 mL two-necked round bottom flask with a reflux condenser were placed **6** (4.34 g, 10.0 mmol), **7** (9.72 g, 24.0 mmol), Pd(PPh_3)$_4$ (350 mg, 0.30 mmol) and Na_2CO_3 (3.18 g, 30.0 mmol). The flask was evacuated under vacuum and flushed with dry nitrogen three times and then toluene (70 mL), ethanol (20 mL) and water (10 mL) were added. The reaction mixture was refluxed for 24 h. After cooling to room temperature, the mixture was poured into water and extracted with dichloromethane three times. The combined organic layers were dried over anhydrous magnesium sulfate. After filtration and solvent evaporation, the crude product was purified by silica-gel column chromatography. Yellow solid compound **8** was obtained in 70% yield. ^{1}H NMR (600 MHz, $CDCl_3$), δ (ppm): 7.93 (d, 4H, J = 7.8 Hz), 7.78 (d, 4H, J = 7.8 Hz), 7.65–7.62 (m, 8H), 6.85 (s, 8H), 2.32 (s, 12H), 2.04 (s, 24H). ^{13}C NMR (125 MHz, $CDCl_3$), δ (ppm): 195.79, 145.55, 144.72, 142.93, 141.65, 140.81, 138.78, 137.04, 136.70, 130.66, 128.23, 127.12, 126.76, 23.49, 21.24. HRMS ($C_{61}H_{60}B_2O$): m/z 831.4889 [M^+, calcd 830.4830].

4′,4‴-{2,2-Bis[4′-(dimesitylboranyl)-(1,1′-biphenyl)-4-yl]ethene-1,1-diyl}bis[*N*,*N*-diphenyl-(1,1′-biphenyl)-4-amine] (TPE-2PN2PB) and 1,1,2,2-tetrakis[4′-(dimesitylboranyl)-(1,1′-biphenyl)-4-yl]ethene (TPE-4PB). Into a 250 mL two-necked round-bottom flask with a reflux condenser were placed **8** (4.15 g, 5.0 mmol), **4** (10.03 g, 15.0 mmol) and zinc dust (2.60 g, 40.0 mmol). The flask was evacuated under vacuum and flushed with dry nitrogen three times, and then dry THF (100 mL) was added. After the mixture was cooled to −78 °C, $TiCl_4$ (3.80 g, 20.0 mmol) was then added dropwise by a syringe. After stirring for 15 min at −78 °C, the mixture was slowly warmed to room temperature and then was heated to reflux overnight. The mixture was quenched with 10% aqueous sodium carbonate and extracted with dichloromethane three times. The combined organic layers were washed with water and dried over anhydrous magnesium sulfate. After filtration and solvent evaporation, the crude product was purified by silica gel column chromatography. Yellow solids TPE-2PN2PB and TPE-4PB were obtained in 35% and 40% yields, respectively. TPE-2PN2PB: ^{1}H NMR (400 MHz, CD_2Cl_2), δ (ppm): 7.60 (d, 4H, J = 8.4 Hz), 7.52–7.45 (m, 12H), 7.40 (d, 4H, J = 8.0 Hz), 7.29 (t, 8H, J = 8.0 Hz), 7.21–7.16 (m, 8H), 7.11–7.02 (m, 16H), 6.84 (s, 8H), 2.31 (s, 12H), 2.01 (s, 24H). ^{13}C NMR (150 MHz, $CDCl_3$), δ (ppm): 147.66, 147.16, 144.55, 143.66, 143.57, 142.26, 141.78, 140.92, 140.82, 139.99, 138.57, 138.53, 138.39, 137.04, 134.47, 132.02, 131.96, 129.25, 128.16, 127.48, 126.47, 126.21, 125.80, 124.36,

123.96, 122.89, 23.46, 21.22. HRMS ($C_{110}H_{96}B_2N_2$): *m/z* 1467.7769 [M^+, calcd 1467.7793]. TPE-4PB: ^{1}H NMR (600 MHz, $CDCl_3$), δ (ppm): 7.56–7.53 (m, 16H), 7.47 (d, 8H, J = 9.0 Hz), 7.18 (d, 8H, J = 8.4 Hz), 6.82 (s, 16H), 2.31 (s, 24H), 2.01 (s, 48H). ^{13}C NMR (125 MHz, $CDCl_3$), δ (ppm): 144.53, 143.56, 143.32, 141.73, 140.79, 140.52, 138.57, 138.54, 137.04, 131.99, 128.15, 126.52, 126.21, 23.46, 21.22. HRMS ($C_{122}H_{120}B_4$): *m/z* 1629.9822 [M^+, calcd 1629.9796].

[4′-(Dimesitylboranyl)-(1,1′-biphenyl)-4-yl][4′-(diphenylamino)-(1,1′-biphenyl)-4-yl]methanone (11). Into a 250 mL two-necked round bottom flask with a reflux condenser were placed **9** (5.04 g, 10.0 mmol), **10** (4.44 g, 12.0 mmol), $Pd(PPh_3)_4$ (350 mg, 0.30 mmol) and Na_2CO_3 (3.18 g, 30.0 mmol). The flask was evacuated under vacuum and flushed with dry nitrogen three times, and then toluene (70 mL), ethanol (20 mL) and water (10 mL) were added. The reaction mixture was heated to reflux for 24 h. After cooling to room temperature, the mixture was poured into water and extracted with dichloromethane three times. The combined organic layers were dried over anhydrous magnesium sulfate. After filtration and solvent evaporation, the crude product was purified by silica-gel column chromatography. Yellow solid compound **11** was obtained in 80% yield. ^{1}H NMR (600 MHz, $CDCl_3$), δ (ppm): 7.95–7.92 (m, 4H), 7.81 (d, 2H, J = 7.8 Hz), 7.72 (d, 2H, J = 7.8 Hz), 7.68–7.64 (m, 4H), 7.57 (d, 2H, J = 7.8 Hz), 7.33 (t, 4H, J = 8.4 Hz), 7.19 (d, 6H, J = 8.4 Hz), 7.10 (t, 2H, J = 7.2 Hz), 6.87 (s, 4H), 2.35 (s, 6H), 2.07 (s, 12H). ^{13}C NMR (150 MHz, $CDCl_3$), δ (ppm): 195.79, 148.17, 147.44, 145.55, 144.73, 144.58, 143.01, 141.68, 140.84, 138.79, 137.05, 136.94, 135.74, 133.25, 130.78, 130.61, 129.38, 128.24, 127.95, 127.09, 126.76, 126.29, 124.79, 123.36, 123.32, 23.49, 21.24. HRMS ($C_{55}H_{48}BNO$): *m/z* 749.3846 [M^+, calcd 749.3829].

4′-{2,2-Bis(4-bromophenyl)-1-[4′-(dimesitylboranyl)-(1,1′-biphenyl)-4-yl]vinyl}-*N*,*N*-diphenyl-(1,1′-biphenyl)-4-amine (12). Into a 250 mL two-necked round-bottom flask with a reflux condenser were placed **11** (3.75 g, 5.0 mmol), **3** (5.10 g, 15.0 mmol) and zinc dust (2.60 g, 40.0 mmol). The flask was evacuated under vacuum and flushed with dry nitrogen three times, and then dry THF (100 mL) was added. After the mixture was cooled to −78 °C, $TiCl_4$ (3.80 g, 20.0 mmol) was then added dropwise by a syringe. After stirring for 15 min at −78 °C, the mixture was slowly warmed to room temperature and then was heated to reflux overnight. The mixture was quenched with 10% aqueous sodium carbonate and extracted with dichloromethane three times. The combined organic layers were washed with water and dried over anhydrous magnesium sulfate. After filtration and solvent evaporation, the crude product was purified by silica gel column chromatography. Green solid compound **12** was obtained in 47% yield. ^{1}H NMR (600 MHz, $CDCl_3$), δ (ppm): 7.57–7.54 (m, 4H), 7.47 (t, 4H, J = 7.8 Hz), 7.37 (d, 2H, J = 8.4 Hz), 7.27–7.24 (m, 8H), 7.12–7.10 (m, 8H), 7.06–7.01 (m, 4H), 6.93–6.91 (m, 4H), 6.82 (s, 4H), 2.31 (s, 6H), 2.02 (s, 12H). ^{13}C NMR (150 MHz, $CDCl_3$), δ (ppm): 147.62, 147.30, 143.43, 142.73, 142.26, 142.23, 141.47, 141.44, 140.81, 138.92, 138.85, 138.61, 137.04, 134.20, 132.99, 131.80, 131.71, 131.15, 131.12, 129.27, 128.18, 127.50, 126.61, 126.24, 125.93, 124.40, 123.89, 122.95, 120.87, 120.84, 23.46, 21.22. HRMS ($C_{68}H_{56}BBr_2N$): *m/z* 1057.2871 [M^+, calcd 1057.2852].

***N*,*N*-Diphenyl-4′-{1,2,2-tris[4′-(dimesitylboranyl)-(1,1′-biphenyl)-4-yl]vinyl}-(1,1′-biphenyl)-4-amine (TPE-PN3PB).** Into a 250 mL two-necked round bottom flask with a reflux condenser were placed **12** (3.17 g, 3.0 mmol), **10** (4.44 g, 12.0 mmol), $Pd(PPh_3)_4$ (230 mg, 0.2 mmol) and Na_2CO_3 (1.06 g, 10.0 mmol). The flask was evacuated under vacuum and flushed with dry nitrogen three times, and then toluene (70 mL), ethanol (20 mL) and water (10 mL) were added. The reaction mixture was heated to reflux for 24 h. After cooling to room temperature, the mixture was poured into water and extracted with dichloromethane three times. The combined organic layers were dried over anhydrous magnesium sulfate. After filtration and solvent evaporation, the crude product was purified by silica-gel column chromatography. Yellow solid TPE-PN3PB was obtained in 65% yield. ^{1}H NMR (500 MHz, $CDCl_3$), δ (ppm): 7.56–7.53 (m, 12H), 7.47–7.43 (m, 8H), 7.37 (d, 2H, J = 8.0 Hz), 7.27–7.23 (m, 4H), 7.20–7.09 (m, 14H), 7.02 (t, 2H, J = 7.5 Hz), 6.82 (s, 12H), 2.31 (s, 18H), 2.01 (s, 36H). ^{13}C NMR (125 MHz, $CDCl_3$), δ (ppm): 147.62, 147.14, 145.14, 144.50, 143.62, 143.59, 143.43, 142.79, 142.15, 141.73, 141.40, 140.80, 140.71, 140.24, 139.43, 138.56, 138.45, 137.04, 136.37, 134.38, 132.01, 131.92, 129.24, 128.14, 127.47, 126.49, 126.21, 125.81, 124.34, 123.92, 122.88, 23.46, 21.22. HRMS ($C_{116}H_{108}B_3N$): *m/z* 1548.8801 [M^+, calcd 1548.8794].

Acknowledgements

We acknowledge the financial support from the National Natural Science Foundation of China (51273053), the National Basic Research Program of China (973 Program, 2015CB655000 and 2013CB834702), the Guangdong Natural Science Funds for Distinguished Young Scholar (2014A030306035), the Guangdong Innovative Research Team Program of China (201101C0105067115) and the Fundamental Research Funds for the Central Universities (2015PT020).

References

1 C. W. Tang and S. A. VanSlyke, *Appl. Phys. Lett.*, 1987, **51**, 913–915.
2 L. Chen, Y. Jiang, H. Nie, P. Lu, H. H. Y. Sung, I. D. Williams, H. S. Kwok, F. Huang, A. Qin, Z. Zhao and B. Z. Tang, *Adv. Funct. Mater.*, 2014, **24**, 3621–3630.
3 J. Huang, N. Sun, Y. Dong, R. Tang, P. Lu, P. Cai, Q. Li, D. Ma, J. Qin and Z. Li, *Adv. Funct. Mater.*, 2013, **23**, 2329–2337.
4 H. Uoyama, K. Goushi, K. Shizu, H. Nomura and C. Adachi, *Nature*, 2012, **492**, 234–238.
5 S.-J. Su, E. Gonmori, H. Sasabe and J. Kido, *Adv. Mater.*, 2008, **20**, 4189–4194.
6 H. Kim, Y. Byun, R. R. Das, B.-K. Choi and P.-S. Ahn, *Appl. Phys. Lett.*, 2007, **91**, 093512.
7 Z. Ding, R. Xing, Q. Fu, D. Ma and Y. Han, *Org. Electron.*, 2011, **12**, 703–709.
8 D. Wang, Z. Wu, X. Zhang, B. Jiao, S. Liang, D. Wang, R. He and X. Hou, *Org. Electron.*, 2010, **11**, 641–648.

9 A. C. Grimsdale, K. Leok Chan, R. E. Martin, P. G. Jokisz and A. B. Holmes, *Chem. Rev.*, 2009, **109**, 897–1091.
10 F. Huang, L. Hou, H. Wu, X. Wang, H. Shen, W. Cao, W. Yang and Y. Cao, *J. Am. Chem. Soc.*, 2004, **126**, 9845–9853.
11 Z. Chen, C. Jiang, Q. Niu, J. Peng and Y. Cao, *Org. Electron.*, 2008, **9**, 1002–1009.
12 S. Xue, L. Yao, F. Shen, C. Gu, H. Wu and Y. Ma, *Adv. Funct. Mater.*, 2012, **22**, 1092–1097.
13 W. Y. Lai, Q. Y. He, R. Zhu, Q. Q. Chen and W. Huang, *Adv. Funct. Mater.*, 2008, **18**, 265–276.
14 Z. Jiang, T. Ye, C. Yang, D. Yang, M. Zhu, C. Zhong, J. Qin and D. Ma, *Chem. Mater.*, 2011, **23**, 771–777.
15 Q. Fu, J. Chen, C. Shi and D. Ma, *ACS Appl. Mater. Interfaces*, 2012, **4**, 6579–6586.
16 Y. Zhou, Q. He, Y. Yang, H. Zhong, C. He, G. Sang, W. Liu, C. Yang, F. Bai and Y. Li, *Adv. Funct. Mater.*, 2008, **18**, 3299–3306.
17 L. Duan, L. Hou, T.-W. Lee, J. Qiao, D. Zhang, G. Dong, L. Wang and Y. Qiu, *J. Mater. Chem.*, 2010, **20**, 6392–6407.
18 F. Liu, C. Tang, Q.-Q. Chen, F.-F. Shi, H.-B. Wu, L.-H. Xie, B. Peng, W. Wei, Y. Cao and W. Huang, *J. Phys. Chem. C*, 2009, **113**, 4641–4647.
19 L. Chen, Y. Jiang, H. Nie, R. Hu, H. S. Kwok, F. Huang, A. Qin, Z. Zhao and B. Z. Tang, *ACS Appl. Mater. Interfaces*, 2014, **6**, 17215–17225.
20 H. Saigusa and E. C. Lim, *J. Chem. Phys.*, 1995, **103**, 8793–8804.
21 L. Chen, S. Xu, D. McBranch and D. Whitten, *J. Am. Chem. Soc.*, 2000, **122**, 9302–9303.
22 S. Hecht and J. M. J. Fréchet, *Angew. Chem., Int. Ed.*, 2001, **40**, 74–91.
23 C.-T. Chen, *Chem. Mater.*, 2004, **16**, 4389–4400.
24 J. D. Luo, Z. L. Xie, J. W. Y. Lam, L. Cheng, H. Y. Chen, C. F. Qiu, H. S. Kwok, X. W. Zhan, Y. Q. Liu, D. B. Zhu and B. Z. Tang, *Chem. Commun.*, 2001, 1740–1741.
25 Y. Hong, J. W. Y. Lam and B. Z. Tang, *Chem. Commun.*, 2009, 4332–4353.
26 Y. Hong, J. W. Y. Lam and B. Z. Tang, *Chem. Soc. Rev.*, 2011, **40**, 5361–5388.
27 X. Zhang, Z. Chi, H. Li, B. Xu, X. Li, W. Zhou, S. Liu, Y. Zhang and J. Xu, *Chem. – Asian J.*, 2011, **6**, 808–811.
28 B. Xu, J. He, Y. Mu, Q. Zhu, S. Wu, Y. Wang, Y. Zhang, C. Jin, C. Lo, Z. Chi, A. Lien, S. Liu and J. Xu, *Chem. Sci.*, 2015, **6**, 3236–3241.
29 W. Z. Yuan, S. Chen, J. W. Y. Lam, C. Deng, P. Lu, H. H. Y. Sung, I. D. Williams, H. S. Kwok, Y. Zhang and B. Z. Tang, *Chem. Commun.*, 2011, **47**, 11216–11218.
30 Z. Zhao, Z. Wang, P. Lu, C. Y. K. Chan, D. Liu, J. W. Y. Lam, H. H. Y. Sung, I. D. Williams, Y. Ma and B. Z. Tang, *Angew. Chem., Int. Ed.*, 2009, **48**, 7608–7611.
31 X. Zhan, N. Sun, Z. Wu, J. Tu, L. Yuan, X. Tang, Y. Xie, Q. Peng, Y. Dong, Q. Li, D. Ma and Z. Li, *Chem. Mater.*, 2015, **27**, 1847–1854.
32 Z. Zhao, J. W. Y. Lam and B. Z. Tang, *J. Mater. Chem.*, 2012, **22**, 23726–23740.
33 Z. Ning, Z. Chen, Q. Zhang, Y. Yan, S. Qian, Y. Cao and H. Tian, *Adv. Funct. Mater.*, 2007, **17**, 3799–3807.
34 J. N. Moorthy, P. Venkatakrishnan, P. Natarajan, Z. Lin and T. J. Chow, *J. Org. Chem.*, 2010, **75**, 2599–2609.
35 Y. Liu, S. Chen, J. W. Y. Lam, P. Lu, R. T. K. Kwok, F. Mahtab, H. S. Kwok and B. Z. Tang, *Chem. Mater.*, 2011, **23**, 2536–2544.
36 J. Huang, N. Sun, J. Yang, R. Tang, Q. Li, D. Ma and Z. Li, *Adv. Funct. Mater.*, 2014, **24**, 7645–7654.
37 Z. Zhao, C. Deng, S. Chen, J. W. Y. Lam, W. Qin, P. Lu, Z. Wang, H. S. Kwok, Y. Ma, H. Qiu and B. Z. Tang, *Chem. Commun.*, 2011, **47**, 8847–8849.
38 C.-L. Chang, C.-W. Hu, C.-Y. Tseng, C.-N. Chuang, K.-C. Ho and M.-k. Leung, *Electrochim. Acta*, 2014, **116**, 69–77.
39 Y. H. Kim, Q. H. Zhao and S. K. Kwon, *J. Polym. Sci., Part A: Polym. Chem.*, 2006, **44**, 172–182.
40 C. L. Chiang, S. M. Tseng, C. T. Chen, C. P. Hsu and C. F. Shu, *Adv. Funct. Mater.*, 2008, **18**, 248–257.
41 T. Nakabayashi, M. Wahadoszamen and N. Ohta, *J. Am. Chem. Soc.*, 2005, **127**, 7041–7052.
42 H. A. Al-Attar, G. C. Griffiths, T. N. Moore, M. Tavasli, M. A. Fox, M. R. Bryce and A. P. Monkman, *Adv. Funct. Mater.*, 2011, **21**, 2376–2382.
43 J. Y. Li, T. Zhang, Y. J. Liang and R. X. Yang, *Adv. Funct. Mater.*, 2013, **23**, 619–628.
44 Z. Gao, C. S. Lee, I. Bello, S. T. Lee, R.-M. Chen, T.-Y. Luh, J. Shi and C. W. Tang, *Appl. Phys. Lett.*, 1999, **74**, 865–867.
45 L. Duan, J. Qiao, Y. Sun and Y. Qiu, *Adv. Mater.*, 2011, **23**, 1137–1144.
46 T. H. Huang, J. T. Lin, L. Y. Chen, Y. T. Lin and C. C. Wu, *Adv. Mater.*, 2006, **18**, 602–606.
47 Y.-J. Pu, G. Nakata, F. Satoh, H. Sasabe, D. Yokoyama and J. Kido, *Adv. Mater.*, 2012, **24**, 1765–1770.
48 F. Tang, J. Peng, R. Liu, C. Yao, X. Xu and L. Li, *RSC Adv.*, 2015, **5**, 71419–71424.
49 K. T. Kamtekar, C. Wang, S. Bettington, A. S. Batsanov, I. F. Perepichka, M. R. Bryce, J. H. Ahn, M. Rabinal and M. C. Petty, *J. Mater. Chem.*, 2006, **16**, 3823–3835.
50 X.-W. Zhang, J.-Y. Wang, L.-L. Zhao, X. Guo, W.-Y. Lai and W. Huang, *Chin. Phys. Lett.*, 2013, **30**, 98501.
51 Z. Q. Jiang, T. L. Ye, C. L. Yang, D. Z. Yang, M. R. Zhu, C. Zhong, J. G. Qin and D. G. Ma, *Chem. Mater.*, 2011, **23**, 771–777.